Solid State Ionics 429 (2025) 116987

Contents lists available at ScienceDirect

Solid State Ionics

journal homepage: www.elsevier.com/locate/ssi

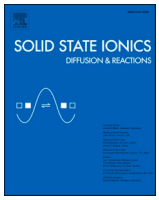

On the interpretation of the impedance response of a passivated lithium metal anode

Sara Drvarič Talian [a], Nejc Urbanija [a], Miran Gaberšček [a,b,*]

[a] Department of Materials Chemistry, National institute of chemistry, Hajdrihova 19, 1000 Ljubljana, Slovenia
[b] Faculty of Chemistry and Chemical Technology University of Ljubljana, Večna pot 113, 1000 Ljubljana, Slovenia

ARTICLE INFO

Keywords:
lithium metal
Solid electrolyte interface
Impedance spectroscopy
Electrolyte concentration
Electrolyte composition
2D impedance model
Equivalent circuit

ABSTRACT

The impedance response of passivated lithium metal anodes has been the subject of numerous studies. However, the exact significance of the main contribution – the mid-frequency arc due to the formation of the solid electrolyte interphase (SEI) - has not been satisfactorily explained. In particular, many studies have pointed to the existence of two closely coupled arcs – instead of one, which further complicates the interpretation. This study systematically investigates the possible underlying processes that determine the impedance characteristics of the SEI using four electrolytes with concentrations ranging from 1 M to 10^{-4} M. The experimental results show that features attributed to processes in the electrolyte phase, such as migration and diffusion, scale significantly with concentration. However, the resistance associated with the coupled mid-frequency arc (the "SEI arc") shows a modest increase, challenging conventional hypotheses. A novel two-dimensional transmission line model is introduced to account for the heterogeneous topology of the SEI and to capture the interplay of liquid and solid phases. The model accurately describes the observed trends over the entire concentration range and reveals the crucial influence of the SEI on the overall impedance. This work provides new insights into the structure-function relationships of the SEI and highlights the need for topology-aware modeling to understand lithium metal anodes.

1. Introduction

Lithium metal is spontaneously passivated when it comes into contact with the environment. The passive film that forms on lithium in organic electrolytes is commonly known as solid electrolyte interphase (SEI) [1]. As the name indicates, this layer conducts ions but is insulating to electrons (similar to liquid electrolytes). The thickness, composition and morphology of the SEI varies considerably depending on the conditions. Authors often report two fundamentally different morphological parts: (i) a very thin (not more than a few nanometers) dense, compact solid structure forms directly on the surface, (ii) a porous structure grows on top of this dense layer and can reach thicknesses of several hundred nanometers [2–7].

The typical impedance response of SEI-covered lithium metal (non-cycled), measured in conventional cells (pouch cells, coin cells, 1 M organic electrolyte), is shown schematically in Fig. 1. Although spectra of similar shape and size have often been reported, the main focus has usually been on the features at the highest to intermediate frequencies, i.e. the features labeled A and B + C in Fig. 1. There seems to be a broad consensus in the literature that the high-frequency intercept on the real axis (feature A) is mainly due to the migration of mobile species in the electrolyte-soaked separator. Similarly, the arc at intermediate frequencies (with a peak frequency in the range of 100–1000 Hz) is usually attributed to the transport of mobile species through the dense, nanometer-thick portion of the SEI. This arc is labeled B + C because a detailed analysis of this apparently »single arc« shows that it actually consists of two closely coupled arcs [8–12] that are difficult to distinguish optically in the complex plane representation. The physical meaning of processes B and C does not seem to be entirely clear. There are at least three possible physical explanations for the occurrence of arc B + C in the literature [8–14]: (i) desolvation of the ions and incorporation into the SEI, (ii) migration of the ions (ionic defects) across the thickness of the SEI, and (iii) the electrochemical reaction (reduction of lithium ions to lithium metal). If this hypothesis is accepted, then the measured spectra could be explained by a combination of two of these three processes, e.g. step (i) and step (ii), while the impedance of the

This article is part of a Special issue entitled: 'Solid State Ionics 100' published in Solid State Ionics.

* Corresponding author at: Department of Materials Chemistry, National institute of chemistry, Hajdrihova 19, 1000 Ljubljana, Slovenia
E-mail address: miran.gaberscek@ki.si (M. Gaberšček).

https://doi.org/10.1016/j.ssi.2025.116987
Received 29 December 2024; Received in revised form 18 June 2025; Accepted 27 July 2025
Available online 31 July 2025

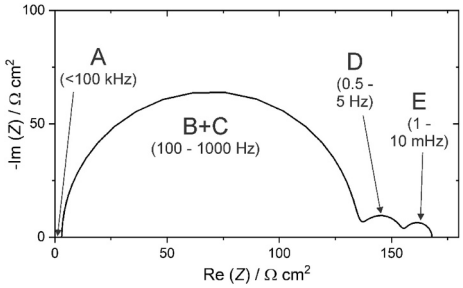

Fig. 1. A typical spectrum of SEI-covered lithium metal before cycling at OCV conditions obtained in a cell with thin separator (on the order of 10 μm) and with conventional concentration of electrolyte (1 M) (the division into sections corresponds to our previous references [3,4]).

third step is assumed to be too small to be detected.

In this paper, we present systematic experiments on the basis of which we propose a modification of the conventional three-process hypothesis to explain the main feature of SEI, i.e., the B + C arc. In the experiments, we systematically vary the concentration of the electrolyte (from 1 M to 10^{-4} M) as well as the composition of the electrolyte (4 different electrolytes are used, as described in the Experimental section). This rather wide variation of conditions also allows a more precise identification of feature D in Fig. 1, which we have already provisionally attributed to the diffusion of mobile species in the thicker, porous part of the SEI [3,4]. Finally, the present measurements also confirm the previously proposed physical meaning of the arc E (usually observed in the 1–10 mHz range), which is attributed to the diffusion of mobile species in the electrolyte-soaked separator (in the present case with a thickness of 20 μm).

2. Experimental

The materials preparation and cell assembly were conducted in an MBRAUN glovebox where the oxygen and water levels were kept below 1 ppm.

LP40 electrolyte (1 M $LiPF_6$ in ethylene carbonate (EC): diethyl carbonate (DEC) 1:1 v:v) was obtained from Elyte innovations and used as is. Lithium bis(trifluoromethanesulfonyl)imide (LiTFSI, Sigma Aldrich, 99.95 %) and lithium bis(fluorosulfonyl)imide (LiFSI, Solvionic, 99.9 %) were dried at 120 °C in vacuum overnight. Li_2S_8 was synthesized by mixing stoichiometric amounts of sulfur (Sigma Aldrich, 99.98 %) and Li (110-μm-thick, FMC) in tetrahydrofuran (THF) until fully reacted and then isolating the powder by heating the mixture under reduced pressure as reported previously [15]. Note that Li_2S_8 powder is not pure, but a mixture of sulfur and polysulfide species with an average oxidation state of Li_2S_8. Tetraglyme (TEGDME, Sigma Aldrich, 99 %), 1,3-dioxolane (DOL, Sigma Aldrich, anhydrous, 75 ppm BHT as inhibitor), dimethoxyethane (DME, Honeywell, 99.9 %), ethylene carbonate (EC, Sigma Aldrich, 99 %) and diethyl carbonate (DEC, Aldrich, 99 %) were dried in the laboratory using a several-step process involving molecular sieves and distillation with Na/K alloy [16]. 2,2-bis (trifluoromethyl) 1,3-dioxolane (BTFD, Apollo Scientific, 99 %) was dried by adding molecular sieves (4 Å) and leaving the mixture inside the glovebox for 7 days. The content of water in all dried solvents was checked using Karl-Fischer (Metler Toledo, C20) inside the glovebox to be below 1 ppm.

The electrolytes were prepared from previously dried salts and solvents by preparing the highest tested electrolyte concentration in a volumetric flask. 1 M LiTFSI in TEGDME:DOL 1:1 (v:v), 1 M LiFSI in BTFD:DME 1:1 (v:v) and 0.8 M Li_2S_8 in TEGDME:DOL 1:1 (v:v) were prepared. The solubility of Li_2S_8 in the TEGDME:DOL 1:1 (v:v) mixture was limited to 0.8 M, so this was used as the highest concentration. An appropriate mass of salt was weighed into the flask. After dissolving the salt in a small amount of solvent mixture, the flask was filled to the marked line with the solvents. Lower electrolyte concentrations were prepared by volumetric dilution in vials – e.g., 0.1 M electrolyte was prepared by diluting 100 μL of the 1.0 M electrolyte with 900 μL of solvent mixture.

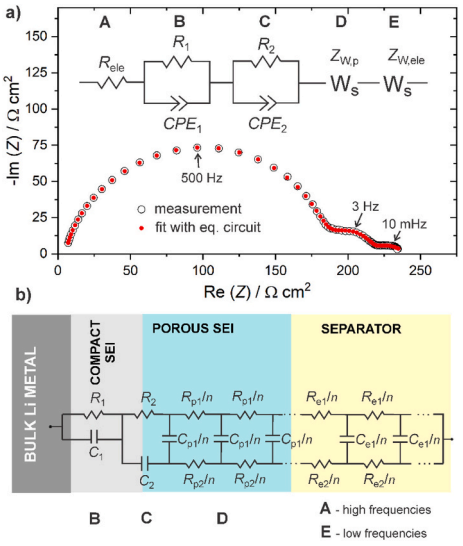

Fig. 2. a) Measured spectrum for 1 M LiFSI in BTFD:DME 1:1 (open black circles; BTFD is a cyclic fluorinated ether, see Experimental section). The frequency range is 20 kHz to 1 mHz. Fit of the measured spectrum using the equivalent circuit shown above the spectrum. The meaning of the circuit elements is explained in the main text. The labels A – E have the same meaning as in Fig. 1. b) Physics based transmission line model (TLM) that fits the measured spectrum with the same accuracy as the equivalent circuit when the capacitors are replaced by CPE elements according to the conventional formula $CPE_i = 1/(j\omega)^{\alpha i}Q_i$: where Q_i replaces the corresponding capacitive element C_i and αi has a value between 0 and 1. The physical meaning of the individual elements in the TLM is discussed in the main text. n is the number of all elements of given type, i.e., it corresponds to the number of planes into which a given phase is divided.

Symmetrical electrochemical cells were assembled using two 2 cm^2 Li metal electrodes punched out of as received Li foil. Two different types of separators were used for cell assembly – Celgard 2320 (18 fi, 20 μm) and GF-A (Whatman, 20 fi, 260 μm). Li|Celgard|GF-A|Celgard|Li cells were assembled by adding 150 μL of only the solvent mixture without the salt (i.e, TEGDME:DOL 1:1 (v:v), BTFD:DME 1:1 (v:v) or EC:DEC 1:1 (v:v)). The cell stack was packaged inside a triplex pouch cell using Ni current collectors. The cells were left to rest at OCV for 10–14 days to enable SEI formation on the electrodes. After that, the cells were opened inside the glovebox and the GF-A separator was removed while at the same time ensuring that the Celgard separators did not detach from the Li metal electrodes. A pristine GF-A separator was then added together with an additional 120 μL of electrolyte of choice. Potentiostatic EIS spectra were measured on the cells using VMP-3 potentiostat/galvanostat (Bio-Logic) at 0 V vs. ref. and 10 mV (rms) amplitude in the frequency range of 20 kHz–1 mHz.

3. Results and discussion

3.1. Effect of electrolyte concentration on the impedance response of passivated lithium

Fig. 2a shows the measured impedance spectrum of a symmetrical Li-Li pouch cell containing 1 M LiFSI in BTFD:DME 1:1 (v:v) as the electrolyte (open black circles). Similar shapes and sizes of impedance spectra were obtained for all 4 electrolytes used in this study when their concentration was 1 M. It can be seen immediately that the shape follows very well the typical schematic spectrum plotted in Fig. 1, except

that the arcs are slightly flattened (depressed) and there is some experimental noise seen, especially at the lowest frequencies.

The measured spectrum can be very well fit with the arbitrary equivalent circuit shown in the inset of Fig. 2a. The elements of this circuit have been chosen so that they roughly correspond to their hypothetical meaning, i.e. to the meaning of sections A-E discussed in the context of Fig. 1. Thus the impedance due to migration of mobile species in the electrolyte is represented with resistor R_{ele}, the coupled processes B and C, which arise from the complex migration across the entire SEI, are represented with resistors R_1 and R_2 in parallel with the corresponding constant phase elements CPE_1 and CPE_2, respectively (the correlation between *CPE* and true capacitor is explained in the caption to Fig. 2). Finally, the diffusion processes in the porous part of SEI and in the electrolyte in separator are described with two respective »Warburg short« elements:

$$Z_w = \left(R_w \tanh(j\omega T)^P\right)/(j\omega T)^P \quad (1)$$

where R_w is the resistance due to diffusion of active species (Li^+), j = $\sqrt{-1}$, ω is the angular frequency of the sinusoidal excitation signal, T is the generalized relaxation time of this diffusion and P is an exponent that mathematically describes the deviation of diffusional impedance from the ideal planar case (for which $P = 0.5$).

Although the equivalent circuit mathematically fits well the measurement, its main role in this paper is primarily to check the number of relaxation processes that are detected in the measured spectrum. Among others, the circuit successfully decouples the processes B + C for which we get the following values of circuit elements: $R_1 = 33\ \Omega$, $R_2 = 141\ \Omega$, $Q_1 = 9.2\text{e-}6\ s^{0.88}\ \Omega^{-1}$, $Q_2 = 5.1\text{e-}6\ s^{0.92}\ \Omega^{-1}$, $\alpha_1 = 0.88$, $\alpha_2 = 0.92$, all normalized per 1 cm^2 of geometric surface area. Similarly, the fitting gives the value of electrolyte resistance (4.9 Ω) and of diffusional elements R_w, T and P which, however, we do not analyze in detail for the reasons stated in next paragraph.

Although mathematical analysis using arbitrary equivalent circuits provides useful information about the number of processes and the typical values of the impedance parameters of a given hypothetical process, a true insight into the physics behind the measured spectra is only possible if we use a physically based modeling of the spectra. An example of such a physical model is the transmission line model (TLM) shown in Fig. 2b, the nature of which has already been discussed in our previous publications [3,4]. Briefly, in the TLM, the movement of a given charge can be traced from one phase to another in a physically accurate way through a sequence of small, localized elements of resistance and capacitance. For example, the path of the Li^+ ion starts in the electrolyte and passes through the resistance elements R_{e1}/n until it reaches the porous part of the SEI, where it »«senses" another local resistance (R_{p1}/n). At the interface between the porous and the compact SEI layer, the Li^+ ion must desolvate and enter the lattice of the SEI, which is considered as the resistance R_2. The average resistance created by the movement through the thin solid SEI finally gives R_1. A similar path can be followed by the inactive mobile counterions, i.e. the mobile anions of the given salt (see the lower branch of the TLM in Fig. 2b). The main difference with respect to the Li^+ ion is at the interface between the porous and the compact SEI, where the anion cannot penetrate the solid SEI lattice but only depletes (or accumulates) at this interface, which can be seen as the capacitor C_2. The capacitor in the compact layer, C_1, is due to the dielectric properties of this layer. Finally, the capacitive elements between the upper and lower resistive branches (rails) represent the so-called chemical capacitors (C_{p1}/n and C_{e1}/n), which at low frequencies accommodate the concentration fluctuations of the mobile species due to their diffusion in the given phase. The full significance of these elements becomes clear when we analyze the spectra using appropriate physical equations, as shown in continuation.

If the capacitors in the TLM in Fig. 2b are replaced by constant-phase elements, CPE (see explanation in the caption to Fig. 2), the measured spectrum can be fit with the TLM with the same accuracy as with the arbitrary equivalent circuit shown in Fig. 2a. The difference is that the parameter values obtained by fitting with TLM can be used for further physical analysis. For example, when the TLM is derived from Newman's porous electrode theory [17], the values for R_{e1}, C_{e1} and R_{e1} can be used to calculate the transport number of lithium ions, t_+, the effective conductivity of the electrolyte, κ_e^{eff}, and the diffusion coefficient of the lithium ion, D_e^{eff}, using the following relationships:

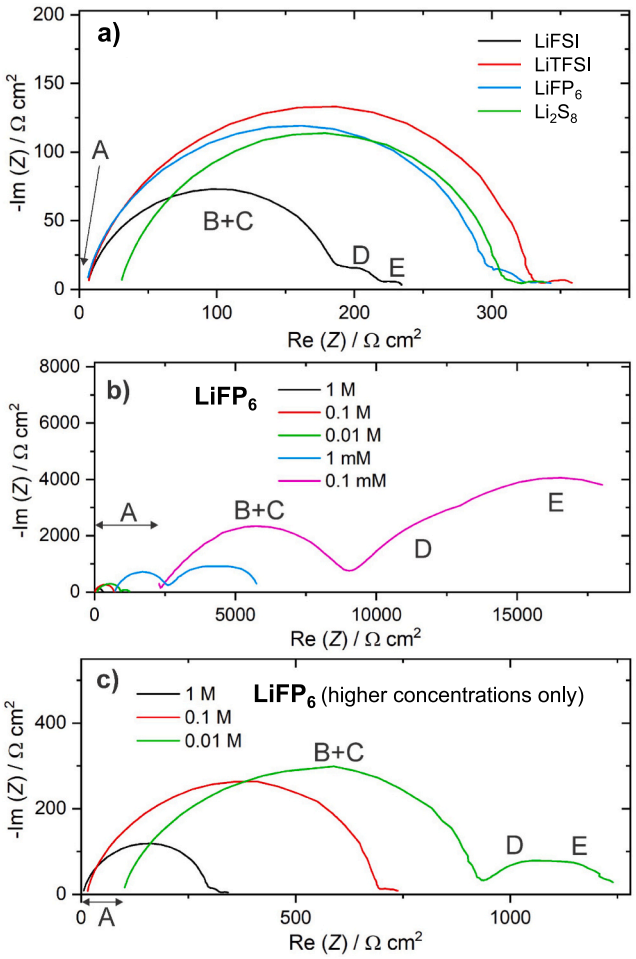

Fig. 3. a) Measured spectra for symmetrical Li-Li cells in 4 different electrolytes with the highest concentrations in this study (1 M except for Li_2S_8, where a concentration of 0.8 M was used instead). B) Measured impedance spectra for cells with the $LiPF_6$ electrolyte at different concentrations: 1 M, 0.1 M, 0.01 M, 1 mM and 0.1 mM. c) The same plots as in panel (b), but for clarity only the smallest plots (highest concentrations) are shown.

$$R_{e1} = \frac{L}{A\kappa_e^{eff} t_+} \quad (2)$$

$$C_{e1} = \frac{AL\varepsilon\kappa_e^{eff}(1-t_+)t_+}{D_e^{eff}} \quad (3)$$

$$R_{e2} = \frac{L}{A\kappa_e^{eff}(1-t_+)} \quad (4)$$

where L is the thickness of the electrolyte-soaked separator, A is the electrode surface area, and ε is the porosity of the separator. Similarly, the same analysis can be performed for the porous part of the SEI or for any other parameter that is part of the given physics based TLM, as shown in our previous publications [17–19].

In order to generalize the present results, we use 4 different electrolytes. Here we must emphasize that in all cases the SEI films were

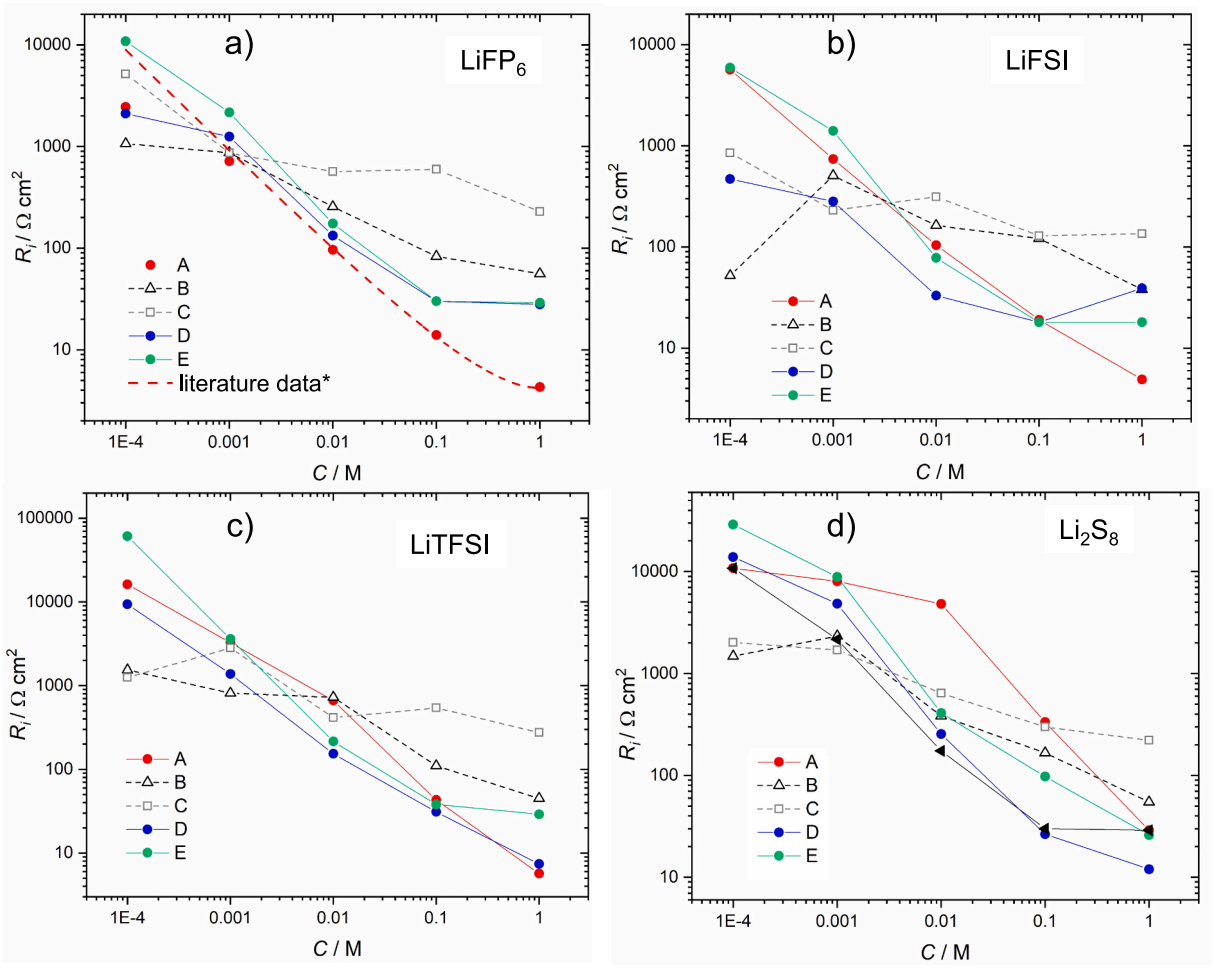

Fig. 4. Resistance of features A-E as a function of concentration of electrolyte calculated from the measured impedance spectra based on equivalent circuit shown in Fig. 2a. a) $LiPF_6$, b) LiFSI, c) LiTFSI and d) Li_2S_8. *In panel a) the results of previous measurements of the conductivity of $LiFP_6$ (ref. [20]) are inserted as red dashed curve and denoted as "literature data". In all cases, the standard deviation of the parameter R_i typically ranged between 15 % and 20 % of its mean value. (For interpretation of the references to colour in this figure legend, the reader is referred to the web version of this article.)

grown in cells containing only the corresponding solvents. After 1–2 weeks of passivation under OCV conditions, the central separator (GF-A separator) was removed and a new separator impregnated with the final electrolyte formulation was added (see Experimental section).

The first aim of this work is to confirm that the TLM presented above adequately describes the measured spectra under all conditions investigated (i.e. at all concentrations and for all 4 electrolytes). The second objective is to find a consistent physical explanation for the coupled features B and C (which are therefore referred to as B + C). Indeed, as far as B + C is concerned, the processes proposed in Fig. 2b are only a theoretical possibility that has not yet been sufficiently tested experimentally. However, if the present hypothesis is correct, i.e. that B is related to processes within the solid part of the SEI and C is related to the insertion of charge from the electrolyte into the SEI, then process B should not depend on the electrolyte concentration, while process C should depend significantly on the electrolyte concentration.

The main idea is therefore to measure the impedance spectrum of the symmetrical Li-Li cell as a function of the electrolyte concentration and to check the dependence of the B + C characteristics on the electrolyte concentration. Of course, the trends for the other characteristics (A, D and E) could also be checked at the same time and their physical origin confirmed.

Fig. 3 shows that the spectra of all 4 cells are similar in shape and size. Essentially all 5 features (A-E) are seen in all 4 cells, although occasionally a particular feature is less pronounced (for example, features D and E are less pronounced in Li_2S_8 and LiTFSI).

The effect of decreasing electrolyte concentration on the impedance spectrum is shown on the example of $LiPF_6$ electrolyte (Fig. 3b and c). It appears that the size of all features increases with decreasing electrolyte concentration. To get a more quantitative description of this dependency, we first analyzed the spectra in Fig. 3b using the simple mathematical equivalent circuit in Fig. 2a. The sizes of features A-E are described with the values of the corresponding fitted resistances which are shown in Fig. 4 for all electrolytes and all concentrations.

All graphs in Fig. 4 show the log-log dependence of the resistance of the respective feature (see Fig. 2a) on the concentration of the 4 electrolytes investigated. For phases containing a liquid electrolyte (separator, porous SEI film), one would expect the conduction to run predominantly through the electrolyte phase, so that a similar dependence on the concentration as for the corresponding bulk electrolyte phase would be expected. Indeed, such agreement can be confirmed by comparing the present result for feature A in LFP (migration resistance through the separator, red dots in Fig. 4a) with previous measurements of the conductivity of LFP6 [20] (red dashed curve in Fig. 4a). We can see that the red dots deviate from the previously reported dashed line only at the lowest concentration (10^{-4} M). We attribute this deviation (which can also be observed in selected other curves in Fig. 4) to experimental uncertainties due to the replacement of the middle separator after aging. As described in Experimental, we used three separators during initial cell assembly and aging, all of which were soaked with the

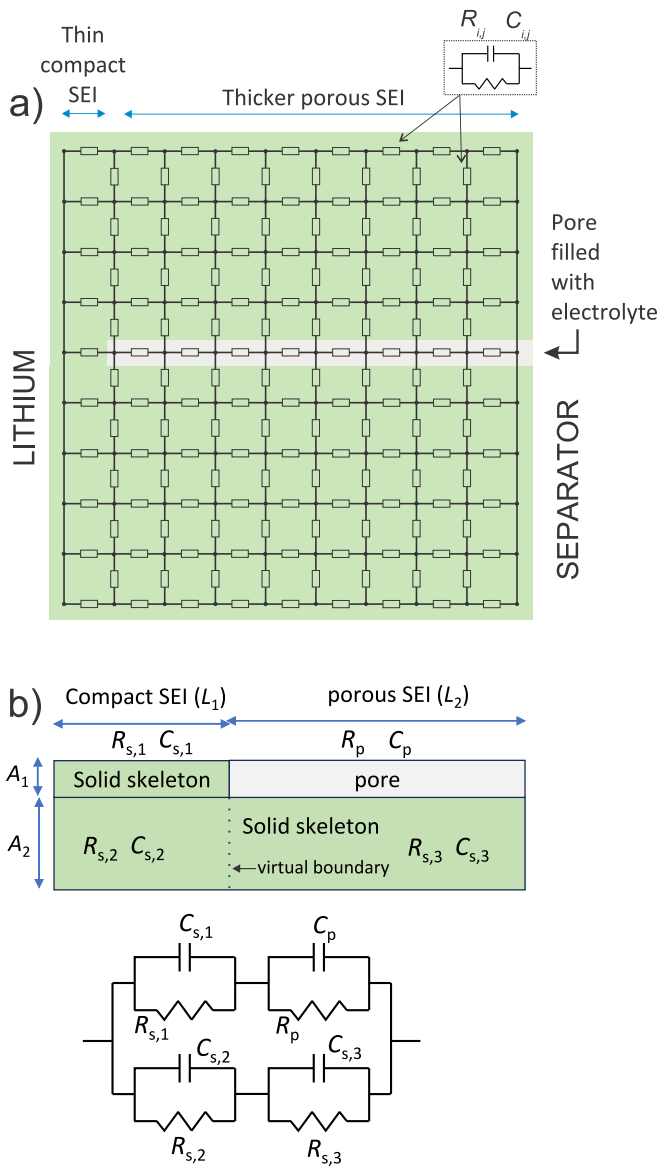

Fig. 5. a) 2D TLM that can explain the occurrence of the closely coupled feature B + C (see Figs. 1–3) in the measured impedance spectra of all 4 electrolytes and all concentrations studied. To illustrate the main concept as simply as possible (and to facilitate further discussion), only one pore is inserted in the solid skeleton in the porous part of the SEI. All elements of the 2D TLM consist of a parallel combination of a resistor and a capacitor, as shown in the upper part of the schematic. The resistor describes the migration of mobile charges in a given phase (either solid or liquid), while the capacitor describes the dielectric properties of the corresponding phase. b) Simplification of the 2D-TLM for cases where the impedance of the vertical elements (i.e. the elements running parallel to the electrode surface) is very high compared to the impedance of the horizontal elements running perpendicular to the electrode surface. Such a situation occurs when the pores are relatively far apart (i.e. in the case of low film porosity). The meaning of the elements in the simplified equivalent circuit is explained graphically in the scheme in panel b) above.

solvent only. Then only the middle separator was replaced with one that was soaked with the actual salt-containing electrolyte. Even if the replaced separator was much thicker, there could still be some dilution of the salt in the remaining thinner separators. This dilution would be relatively greatest in the case of the lowest salt concentration. Another important source of error could be the welding of the coffee bag, where the cell is exposed to very low pressure, which means that some of the solvent could evaporate uncontrollably.

In general, however, it can be safely asserted that most of the curves corresponding to features A, D and E show the typical behavior expected for the dependence of the resistance of the electrolyte on its concentration. This can be interpreted as an indirect confirmation of the original hypothesis regarding the origin of features A, D and E: (i) migration in the electrolyte-soaked separator, (ii) diffusion of mobile species within the electrolyte-filled pores of the porous SEI and (iii) diffusion of mobile species in the electrolyte-soaked separator, respectively.

In contrast, different behavior was observed for features B and C (black and grey triangles and squares). For B, the increase in resistance during the transition from 1 M to 10^{-4} M is typically between 20 and 30 times, while this increase is even lower for feature C: 4–7 times. This much smaller effect of electrolyte concentration is to be expected, as our original hypothesis attributes these two features to processes within the SEI, which consists mainly of solid structures (compact part and porous part, see Fig. 2b). In fact, if we recall the most important assumptions for the physical explanation of feature B + C, we expect that no more than one of the two processes depends on the electrolyte concentration.

3.2. *Comparison of experimental results with TLM-based simulations*

As briefly mentioned in the Introduction, the three possibilities to explain the B + C arc are [8–12]: (a) electrochemical reaction at the interface between Li and solid SEI, (b) migration through the compact solid SEI film, and (c) desolvation/solvation process at the interface between solid SEI and electrolyte. Obviously, of these three possibilities, only process (c) depends on the concentration of the electrolyte.

However, observation of the resistance trends in Fig. 4 shows that both processes B and C change significantly with electrolyte concentration, although the dependence for process C is generally weaker. Since the existing hypotheses on the significance of feature B + C proved to be inconsistent with the trends observed in Fig. 4 for all four electrolytes, we looked for an alternative explanation for the measured behavior. Somewhat surprisingly, we found that even the basic concept of a two-layer SEI - consisting of the transport of ions through a compact solid layer and a porous layer - can explain the observed trends. However, to model this accurately, we need to account for the unique topology of the two-layer structure, which requires the construction of at least a two-dimensional impedance model. This is essential for properly capturing the inhomogeneities arising from the interpenetration of the two phases, which have vastly different conductivities (with the conductivity of the liquid electrolyte being several orders of magnitude higher than that of the solid phases). A two-dimensional model that addresses these factors is presented in Fig. 5a. This model builds upon previous similar approaches, such as those used to describe poor contact at solid-solid interfaces [21]. In the following, we provide a detailed explanation of the main characteristics of this model and propose a simplified version for the specific case of current interest.

The proposed 2D model (Fig. 5a) describes the transport impedance due to migration in both the compact and porous layers of the SEI. The unit element of this migration impedance consists of a migration resistance parallel to the dielectric capacitance (see the dashed rectangle with elements $R_{i,j}$, $C_{i,j}$ at the top of Fig. 5a) at any point in the heterogeneous SEI layer. Since we have only two different materials (solid SEI structure and liquid electrolyte), there are also only two different values for the local $R_{i,j}$, $C_{i,j}$. To illustrate the effect of the interpenetrating phases on the impedance as clearly as possible, we introduce only one pore into the otherwise uniform solid SEI structure, which has a cross-section an order of magnitude larger than the pore (i.e., it spans 9 rows). Such a topology mimics a porous layer with low porosity. The division into two parts (compact and porous) is due to the fact that the pore does not extend to the lithium, but ends at the “apparent location” where the compact layer begins. On the right-hand side of the scheme, however, the pore is in contact with the bulk electrolyte in separator.

The impedance spectra of the 2D model shown in Fig. 5 can be calculated using the Kirchoff’s rules for calculation of currents at all

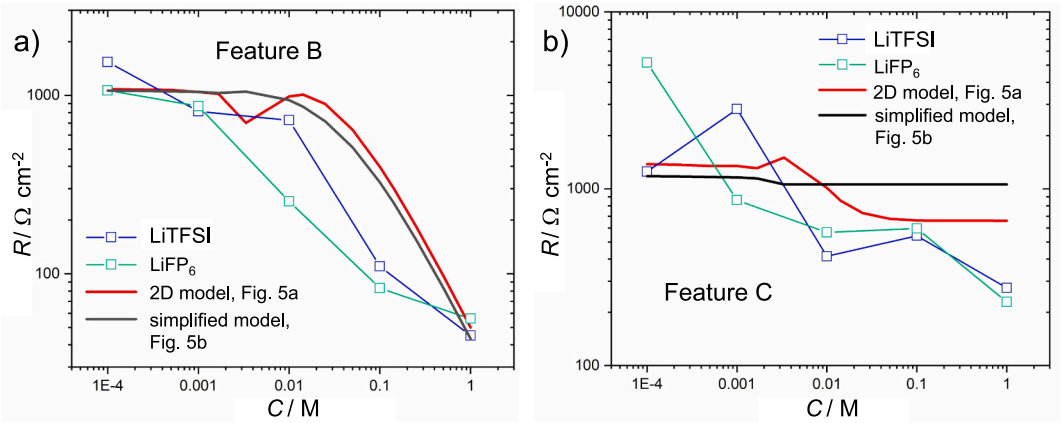

Fig. 6. Comparison of the measured dependence of features B (panel a) and C (panel b) with the model predictions. The same values as in Fig. 4 a) and b) were used for the measured data (blue and green squares). The red model curve was generated with the full 2D model in Fig. 5a, while the black curve was generated with the simplified model in Fig. 5b (both cases, the modeling results were multiplied by two to account for the symmetric cell configuration used in the experiments). Exactly the same parameter values were used for both models and for both features. While the magnitude and the main trends are the same for both models, some obvious differences can be observed, which are explained in the main text. The values of *Ri,j* and *Ci,j* for the elements in 2D model shown in Fig. 5a were as follows. Compact SEI: *R_compact* = 2500 Ω, *C_compact* = 1e-6 F; the same values were used for the solid skeleton of porous SEI: *R_skeleton* = 2500 Ω, *C_skeleton* = 1e-6 F; for the liquid-filled pore in porous SEI the values were: *R_pore* = 10 Ω (for 1 M electrolyte), *C_pore* = 8e-10 F. *R_pore* for lower concentrations was increased proportionally to the measured increase in resistance of the bulk electrolyte (see Fig. 4, feature A - red dots). From the values for the 2D model, one can readily calculate the corresponding values for the parameters of the simplified model in Fig. 5b by taking into account the geometries of both models (i.e. the number of rows and columns in the 2D model need to be properly translated into the ratios between A_1 and A_2 and L_1 and L_2). (For interpretation of the references to colour in this figure legend, the reader is referred to the web version of this article.)

potential nodes (in our case 80 nodes, i.e. points that separate the 162 basic elements). Importantly, such calculation also allows the calculation of all potentials and all currents for any chosen frequency. We will present a couple of such calculations in continuation.

The detailed examination of the properties of the 2D model in Fig. 5a has shown that in some cases the model can be simplified to the conventional 1D sub-cases, as shown in Fig. 5b. For example, this simplified model produces similar impedance spectra to the 2D model when the pores are very far apart (with respect to their thickness) or when the conductivity of the electrolyte in the pores is not too different from the conductivity of the solid part of the SEI. More important for the present context is the fact that the simplified model predicts similar trends as the full 2D model – even if the conductivities of the phases are very different and the pores are relatively close to each other. Both models are used for the preliminary analysis shown in continuation. At this point, it is important to point out that further simplifications of the equivalent circuit in Fig. 5b (e.g. as recently proposed Lim et al. [22]) may not capture the essence of the physical picture at hand, namely the interplay of transport through liquid and solid phases forming the compact and the porous part of the SEI layer, and the resulting strongly coupled two arcs in the complex plane.

Before proceeding, it is important to emphasize that the main drawback for using the proposed models (either 2D or the more conventional 1D variant) in the current context and state of knowledge is that the actual topology of the pores/solids is largely unknown. In other words, we do not know the dimensions of the pores, their location, density, connectivity, etc. Similarly, we know little about the overall thickness of the SEI layer and the individual thicknesses of the individual layers. All these factors have a major influence on the values and shapes of the calculated impedance spectra.

However, despite the lack of precise parameter values and the topology of compact and porous SEI films, the model can be used for a general prediction of parameter trends when the electrolyte concentration is changed by many orders of magnitude. Examples of such trends for the magnitude (resistance) of feature B and C are shown in Fig. 6. For feature B, we can see that the main trend of increasing resistance with decreasing concentration and subsequent plateau of resistance is well reproduced by both models (see the red and black curves for the full and simplified models in Fig. 6a). However, in the case of feature C, the prediction of both models is slightly different: while the full 2D model (red curve) is able to reproduce the increasing trend of the resistance when the electrolyte concentration changes from high to low, this is not the case for the simplified model (black curve) (more precisely, this increase is almost negligible in the log-log plot for the black curve).

We note that although certain experimental trends in Fig. 6 are not fully captured by the proposed model, it is important to emphasize that (i) this is the first study to clearly identify features B and C in a general manner—across different electrolytes and over a wide concentration range—and (ii) the proposed model provides a reasonable approximation of the significant changes in resistance associated with both features. To our knowledge, no existing model more accurately reproduces the observed behavior.

3.3. *Potential and current distributions within the porous SEI*

To better understand the physical origin and coupling between processes B and C, we performed a series of further simulations in which we studied the potential and current distribution in the compact-porous SEI system. An example of such a study can be seen in Fig. 7, which uses the same main topology (one pore leading from the electrolyte to the beginning of the compact layer) as the model in Fig. 5. As expected, it can be seen that the presence of a highly conductive pore filled with electrolyte changes both the potential and current distribution in the near region of the solid part of the porous SEI. This means that the pore "apparently increases" the intrinsic conductivity of the solid skeleton of the porous SEI locally. Importantly, this effect only occurs in the 2D (or a further upgraded 3D) model, whereas in the 1D simplification the distribution of the electric field within the pore and in the surrounding solid part is homogeneous everywhere. This difference explains the difference in the prediction for feature C (and to some extent also feature B) in Fig. 6b.

Despite some differences between the 2D model and the simplified model, it is important to reiterate that both are able to accurately fit the main shape of feature B + C (closely coupled arc). This fact is not necessarily intuitive because, as explained several times, the model includes two different phases with extremely different conductivities: a

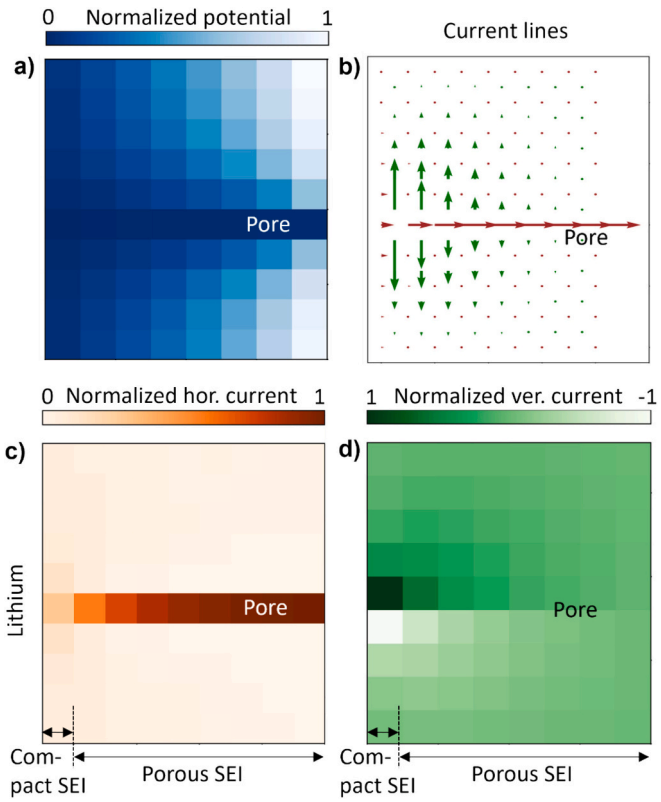

Fig. 7. Calculated potentials and current values at quasi d.c. current conditions (frequency = 10^{-10} Hz). For calculation, the model in Fig. 5a was used and the values of model elements were the same as those used for creation of Fig. 6b. a) Potential values for all 80 nodes in Fig. 5a. b) Calculated current values between all 80 nodes (in both horizontal and vertical direction). Note that for better visualization, the values for green vertical lines are multiplied with 7 with respect to brown horizontal ones (because the average values of the horizontal currents are much bigger). c) Heat map for horizontal currents and d) heat map for vertical currents. In both cases, the currents were normalized such that the highest value was set to 1, the lowest to 0, and all intermediate values were scaled linearly in between. (For interpretation of the references to colour in this figure legend, the reader is referred to the web version of this article.)

liquid electrolyte and a solid conductor for Li ions. Large differences in conductivity mean large differences in relaxation time, so the contribution of the two phases should be well separated (two arcs far away from each other). The fact that they are coupled is relatively easy to understand from the simplified model in Fig. 5b. We see that the impedance of the pore (Rp, Cp) is in series with the underlying compact layer (Cs,1, Rs1), but parallel with the rest of the compact layer (parameters with index 2) and the solid skeleton of the porous layer (parameters with index 3). This mixed series-parallel combination leads to special "interactions" of elements, the result of which tend to be closely coupled arcs such as feature B + C. These special interactions are due to the fact that with resistors in series the larger resistance predominates, while with parallel connection the smaller resistance predominates. The reverse is true for capacitors. Unfortunately, these different connections also mean that, unlike in many other cases, we cannot simply decouple the equivalent circuit diagram in Fig. 5b into two RC terms in series, as is done mathematically in Fig. 2a. In other words: If the model in Fig. 5 is correct, then the RC terms for features B and C in Fig. 2 have no clear physical meaning (although they are mathematically able to fit the spectrum).

On the other hand, fitting with the physical model in Fig. 5 can be challenging because the model is mathematically over-parameterized (there are too many parameters that cannot be uniquely determined by a single fit). In this case, the correct approach would be to measure the impedance response in different series of measurements and determine the unknown parameters from a batch fit (similar to the example of the series of measurements with different electrolyte concentrations in this study, but including additional crucial data, in particular those on the geometry of the layers).

On a more practical note, researchers are often primarily interested in the total resistance of the SEI, as this can serve as a measure of the electrochemical performance of the lithium electrode. As already explained several times, graphically this total resistance is nothing other than the sum of the sizes of B + C arcs. Let us now relate this graphical representation to the parameters that play a role in both the complete (2D) and the simplified model in Fig. 5a and b. For the 2D model, the exact calculation of the total resistance is quite complex and should be done numerically using the model. However, for the simplified model, which applies to the case of low porosity (more precisely, when the distance between the pores is much larger than their typical width), the total resistance corresponding to the size of the B + C features reads:

$$R_{tot} = \frac{(R_{s,1} + R_p)(R_{s,2} + R_{s,3})}{(R_{s,1} + R_p) + (R_{s,2} + R_{s,3})} \quad (5)$$

From Fig. 3, for example, we can see that the typical value of R_{tot} in a symmetrical cell configuration is between 200 and 300 Ω cm^{-2}. Fitting the corresponding arcs using the present model shows that the individual contributions for the different resistors are in the following ranges: $R_{s,1}$ = 400–600 Ω cm^{-2}, R_p = 150–220 Ω cm^{-2}, $R_{s,2}$ = 55–80 Ω cm^{-2} and $R_{s,3}$ = 200–300 Ω cm^{-2}. Contrary to the conventional assumption that only the resistance of the compact film, $R_{s,2}$, contributes to the resistance of the arc B + C, we see that the other contributions are equally, if not more, important. In any case, this result clearly shows that the porous film is not "transparent", but has a significant influence on the overall resistance of feature B + C.

4. Conclusion

We have shown the dependence of the most important impedance characteristics of a passivated lithium anode on the electrolyte concentration. Passivation was performed spontaneously (chemically) by exposing Li to different solvents for about two weeks. Subsequently, the previous middle separator in symmetric Li-Li cells was replaced by a separator impregnated with an electrolyte of a specific concentration. Four different electrolytes in concentration ranges from 1 M to 10^{-4} M were used.

The analysis showed a significant (several orders of magnitude) increase in the magnitude of three (out of 5) impedance characteristics (features) as the electrolyte concentration decreased. This was expected as all three features are due to processes in the electrolyte phase that depend on the concentration: (i) migration in the bulk electrolyte (high frequency feature A), (ii) diffusion in the pores of the porous passive film (feature D) and (iii) diffusion in the bulk electrolyte (feature E). In contrast, the resistance of the main arc (feature B + C) increased much less than the other features: about 5–30 times as opposed to the approximately 1000-fold (or more) increase in electrolyte resistance. To explain this small (but non-negligible) dependence on the electrolyte concentration, we proposed a model that takes into account the main topology of the solid electrolyte interface (thin compact layer on which a much thicker, porous layer grows). To model the impedance of such a topology, we introduced a 2D transmission line model that takes into account the special effects due to the presence of two phases with very different conductivity in the porous structure. The model satisfactorily explains the observed trends in the main arc B + C in the entire concentration range investigated (4 decades). To simplify the implementation of the 2D model, we have also proposed a simplification that captures all the main features of the model. It should be noted that this simplified model works well when porosity is low and is less suitable for highly porous films – in which case the full 2D model must be used. In

any case, to explain the two closely coupled processes, which can be seen as a coupled main arc B + C, one does not need to introduce a special step (e.g. charge transfer reaction, desolvation and incorporation of Li, etc.), since the generally accepted two-layer SEI structure (compact + porous layer) already yields such a coupled arc.

CRediT authorship contribution statement

Sara Drvarič Talian: Writing – review & editing, Data curation, Conceptualization. **Nejc Urbanija:** Validation, Data curation. **Miran Gaberšček:** Writing – review & editing, Writing – original draft, Methodology, Funding acquisition, Formal analysis, Conceptualization.

Declaration of competing interest

The authors declare the following financial interests/personal relationships which may be considered as potential competing interests:

Miran Gaberscek reports financial support was provided by Slovenian Research and Innovation Agency. If there are other authors, they declare that they have no known competing financial interests or personal relationships that could have appeared to influence the work reported in this paper.

Acknowledgments

The authors thank the Slovenian Research and Innovation Agency for funding through research program P2-0393.

Data availability

Data will be made available on request.

References

[1] E. Peled, S. Menkin, SEI: past, present and future, J. Electrochem. Soc. 164 (2017) A1703, https://doi.org/10.1149/2.1441707jes.
[2] X. Yua, A. Manthiram, Electrode–electrolyte interfaces in lithium-based batteries, Energy Environ. Sci. 11 (2018) 527–543, https://doi.org/10.1039/C7EE02555F.
[3] M. Adamič, S. Drvarič Talian, A.R. Sinigoj, I. Humar, J. Moškon, M. Gaberscek, A transmission line model of electrochemical cell's impedance: case study on a Li-S system, J. Electrochem. Soc. 166 (2019) A5045–A5053, https://doi.org/10.1149/2.0061903jes.
[4] S. Drvarič Talian, J. Bobnar, A.R. Sinigoj, I. Humar, M. Gaberšček, Transmission line model for description of the impedance response of Li electrodes with dendritic growth, J. Phys. Chem. C. 123 (2019) 27997–28007, https://doi.org/10.1021/acs.jpcc.9b05887.
[5] Siqi Shi, Lu Peng, Zhongyi Liu, Yue Qi, Louis G. Hector Jr., Hong Li, J. Harris Stephen, Direct calculation of Li-ion transport in the solid electrolyte interphase, J. Am. Chem. Soc. 134 (37) (2012) 15476–15487, https://doi.org/10.1021/ja305366r.
[6] Lu Peng, Chen Li, Eric W. Schneider, Stephen J. Harris, Chemistry, impedance, and morphology evolution in solid electrolyte interphase films during formation in Lithium ion batteries, J. Phys. Chem. C 118 (2) (2014) 896–903, https://doi.org/10.1021/jp4111019.
[7] Rikuya Ito, Hiroki Nara, Toshiyuki Momma, Electrochemical impedance spectroscopy analysis of dendrite growth on the Lithium metal surface in polysulfide-insoluble electrolytes, J. Electrochem. Soc. 171 (2024) 120511, https://doi.org/10.1149/1945-7111/ad9a7e.
[8] J. Huang, Y. Gao, J. Luo, S. Wang, C. Li, S. Chen, J. Zhang, J. Electrochem. Soc. 167 (2020) 166503, https://doi.org/10.1149/1945-7111/abc655/meta.
[9] P.M. Nogales, S. Lee, S. Yang, S.-K. Jeong, Understanding the impact of Li2CO3 distribution within solid electrolyte interphases on lithium metal via thermal conditioning, Electrochim. Acta 503 (2024) 144834, https://doi.org/10.1016/j.electacta.2024.144834.
[10] Peng Gao, Cuifen Zhang, Guangwu Wen, Equivalent circuit model analysis on electrochemical impedance spectroscopy of lithium metal batteries, J. Power Sources 294 (2015) 67–74, https://doi.org/10.1016/j.jpowsour.2015.06.032.
[11] B. Wu, J. Lochala, T. Taverne, J. Xiao, The interplay between solid electrolyte interface (SEI) and dendritic lithium growth, Nano Energy 40 (2017) 34–41, https://doi.org/10.1016/j.nanoen.2017.08.005.
[12] F. Single, B. Horstmann, A. Latz, Theory of impedance spectroscopy for Lithium batteries, J. Phys. Chem. C 123 (2019) 27327–27343, https://doi.org/10.1021/acs.jpcc.9b07389.
[13] Y. Yamada, Y. Iriyama, T. Abe, Z. Ogumi, Kinetics of Lithium ion transfer at the Interface between graphite and liquid electrolytes: effects of solvent and surface film, Langmuir 25 (2009) 12766–12770, https://doi.org/10.1021/la901829v.
[14] Hiroki Nara, Daikichi Mukoyama, Ryo Shimizu, Toshiyuki Momma, Tetsuya Osaka, Systematic analysis of interfacial resistance between the cathode layer and the current collector in lithium-ion batteries by electrochemical impedance spectroscopy, J. Power Sources 409 (2019) 139–147, https://doi.org/10.1016/j.jpowsour.2018.09.014.
[15] Sara Drvarič Talian, Gregor Kapun, Jože Moškon, Alen Vižintin, Anna Randon-Vitanova, Robert Dominko, Miran Gaberšček, Which process limits the operation of a Li–S system? Chem. Mater. 31 (2019) 9012–9023, https://doi.org/10.1021/acs.chemmater.9b03255.
[16] Sara Drvarič Talian, Steffen Jeschke, Alen Vizintin, Klemen Pirnat, Iztok Arčon, Giuliana Aquilanti, Patrik Johansson, Robert Dominko, Fluorinated ether based electrolyte for high-energy Lithium–Sulfur batteries: Li+ Solvation role behind reduced polysulfide solubility, Chem. Mater. 29 (2017) 10037–10044, https://doi.org/10.1021/acs.chemmater.7b03654.
[17] K. Zelič, T. Katrašnik, M. Gaberšček, Derivation of transmission line model from the concentrated solution theory (CST) for porous electrodes, J. Electrochem. Soc. 168 (2021) 070543, https://doi.org/10.1149/1945-7111/ac1314/meta.
[18] J. Moškon, J. Žuntar, S. Drvarič Talian, R. Dominko, M. Gaberšček, J. Electrochem. Soc. 167 (2020) 140539, https://doi.org/10.1149/1945-7111/abc769.
[19] J. Moškon, M. Gaberšček, J. Power Sources Adv. 7 (2021) 100047. https://linkinghub.elsevier.com/retrieve/pii/S2666248521000020.
[20] J. Landesfeind, H.A. Gasteiger, Temperature and concentration dependence of the ionic transport properties of Lithium-ion battery electrolytes, J. Electrochem. Soc. 166 (2019) A3079–A3097, https://doi.org/10.1149/2.0571912jes.
[21] Janis K. Eckhardt, Peter J. Klar, Jürgen Janek, Christian Heiliger, Interplay of dynamic constriction and interface morphology between reversible metal anode and solid electrolyte in solid state batteries, ACS Appl. Mater. Interfaces 14 (2022) 35545–35554, https://doi.org/10.1021/acsami.2c07077.
[22] Kyungmi Lim, Jelena Popovic, Joachim Maier, Ion transport and growth behavior of solid electrolyte interphases on Li and Na with liquid electrolytes based on impedance analysis, J Mater Chem A 11 (2023) 5725, https://doi.org/10.1039/D2TA09189E.